Dual Alternative Iteration Algorithm-based Hierarchical MPC Strategy for Frequency Regulation Control and Active Power Allocation of Wind-storage Coupling System

Zhenhua Cai, Xubin Liu, *Member*, *IEEE*, Canbing Li, *Senior Member*, *IEEE*, Nengling Tai, *Senior Member*, *IEEE*, Wentao Huang, *Senior Member*, *IEEE*, Sheng Huang, and Juan Wei

***Abstract*—This paper proposes a dual alternative iteration algorithm-based hierarchical MPC (DAMPC) strategy to realize frequency regulation control and active power allocation of wind-storage coupling system. The proposed DAMPC strategy involves a top-level grid frequency model predictive control (FMPC) strategy and a bottom-level multi-objective model predictive control (MMPC) strategy. In the FMPC strategy, to improve the frequency regulation performance, the active power reference of the wind-storage coupling system is generated by minimizing the frequency deviation, where the frequency reference is calculated by considering the active power deviation and its integral. In the MMPC strategy, the active power reference is optimally allocated to the wind turbine generators (WTGs) and battery energy storage system (BESS) by raising the minimum rotor speed, minimizing the pitch angle deviation and state of charge (SOC) deviation. To solve the multi-objective allocation optimization problem with high efficiency, a dual alternative iteration algorithm (DAIA) is proposed to update the global and local control vectors with the dual vector. Extensive simulations validate the effectiveness of the proposed DAMPC strategy in frequency regulation and active power allocation.**

***Index Terms*—Wind-storage coupling system, dual alternative iteration algorithm-based hierarchical MPC (DAMPC), grid frequency model predictive control (FMPC), multi-objective model predictive control (MMPC), dual alternative iteration algorithm (DAIA).**

NOMENCLATURE

A. Abbreviations

MPPT	maximum power point tracking
WTG	wind turbine generator
BESS	battery energy storage system
SOC	state of charge
MPC	model predictive control
DAMPC	dual alternative iteration algorithm-based hierarchical MPC
FMPC	grid frequency model predictive control
MMPC	multi-objective model predictive control
DAIA	dual alternative iteration algorithm

B. Variables

f, f_{N}	measured frequency and rated frequency of local power grid
P_{WS}, P_{G}	measured active power of wind-storage coupling system and conventional generator
$\Delta P_{\mathrm{WS,ref}}$	active power reference of wind-storage coupling system
$\Delta P_{\omega,\mathrm{ref},i}$, $\Delta P_{\theta,\mathrm{ref},i}$	rotor speed regulating active power reference and pitch angle regulating active power reference of WTG i
$\Delta P_{\xi,\mathrm{ref}}$	active power reference of BESS
P_{L}, P_{LN}	measured active power load and rated active power load

Received: December 20, 2024
Accepted: July 21, 2025
Published Online: November 1, 2025

Zhenhua Cai is with the College of Electrical and Information Engineering, Hunan University, Changsha 410082, China; and also with the Key laboratory of Energy Monitoring and Edge Computing for Smart City of Hunan Province, Hunan City University, Yiyang 413000, China (e-mail: 403739239@qq.com).

Xubin Liu (corresponding author) is with the School of Automation, Central South University, Changsha 410083, China (liuxubin@csu.edu.cn).

Canbing Li, Nengling Tai, and Wentao Huang are with the School of Electronic Information and Electrical Engineering, Shanghai Jiao Tong University, Shanghai 200240, China (e-mail: licanbing@sjtu.edu.cn; nltai@sjtu.edu.cn; hwt8989@sjtu.edu.cn).

Sheng Huang and Juan Wei are with the College of Electrical and Information Engineering, Hunan University, Changsha 410082, China (e-mail: huang98123@163.com; weijuanba@hnu.edu.cn).

DOI: 10.23919/PCMP.2024.000470

H_{G}, H_{W}	grid inertia constant and WTG rotation inertia constant
D_{F}, T	grid frequency damping factor and time delay of electromechanical power conversion
τ_{θ}, τ_{ω}, τ_{ξ}	time delay of pitch angle regulation, time delay of active power regulated by rotor speed, time delay of active power regulated by BESS
T_{F}, T_{R}, T_{θ}, T_{S}	grid frequency sampling period, rotor speed sampling period, pitch angle sampling period, SOC sampling period
k	time stage
N_{T}, N_{B}	control/prediction time domain of top-level controller and bottom-level controller
f_{ref}, $S_{\mathrm{SOC,ref}}$	frequency and SOC references
K_{D}, K_{I}	droop and inertia coefficients
s	differential operator
$P_{\mathrm{WS,max}}$	maximum active power of wind-storage coupling system
$P_{\xi,\max}$, $C_{\xi,\max}$	maximum charge/discharge power and maximum charge/discharge capacity of BESS
$\Delta P_{\omega,i}$, $\Delta P_{\theta,i}$	rotor speed regulating active power deviation and pitch angle regulating active power deviation of WTG i
ΔP_{ξ}	SOC regulating active power deviation
$\Delta\omega_i$, $\Delta\theta_i$	rotor speed deviation and pitch angle deviation of WTG i
ΔS_{SOC}	state of charge deviation
$\omega_{0,i}$, $P_{\mathrm{m}0,i}$, $P_{\mathrm{e}0,i}$	initial rotor speed, initial mechanical power, and initial active power of WTG i
$P_{\xi,0}$, $P_{\mathrm{WS},0}$	initial active power of BESS and initial active power of wind-storage coupling system
$\Delta P_{\mathrm{m},i}$, $\Delta\theta_{\mathrm{ref},i}$	mechanical power deviation and pitch angle reference deviation of WTG i
k_0	primary term coefficient of pitch angle
ΔP_{int}	integration of difference between $\Delta P_{\xi,\mathrm{ref}}$ and ΔP_{ξ}
δ_{pri}, δ_{dua}	primal and dual thresholds
τ	iteration index

I. Introduction

Significant attention has been given to WTGs through the design of maximum power point tracking (MPPT) control strategies [1]. However, the rapid increase in asynchronous WTGs has reduced the overall inertia support capability of the power system [2]–[4]. BESSs, with their high efficiency, energy density, and fast response, are considered a promising active power resource for frequency regulation in wind farms. Wind-storage coupling system is usually regarded as multiple groups of WTGs integrated with the BESS. In weak grids, a small load disturbance can cause severe frequency fluctuation, or in extreme cases, lead to cascading disconnection of the wind-storage coupling system [5]. In addition, the internal parameter optimization through active power allocation affects the reliability, economic performance, and service life of the system. Therefore, it is imperative to develop an effective active power allocation strategy for wind-storage coupling system during frequency regulation.

To date, extensive research has been conducted on deriving the active power reference command for wind-storage coupling systems under various frequency regulation strategies. The main frequency regulation strategies for active power acquisition include the advanced droop control [6], [7], inertial control [8]–[10], fuzzy control [11], [12] and the prevalent optimal control strategy [13]–[17]. In [8], an adaptive gain frequency control, which exhibits strong robustness to uncertain wind speeds, is proposed for wind power plants to regulate the gains based on the different rotor speeds of the WTGs. In [9], a four-stage transient frequency control of the wind farm is implemented to manage the active power reference according to the stages of the frequency event detection, rotor speed safe recovery, MPPT recovery route selection and implementation. In [10], a hierarchical coordinated inertia control is proposed to improve the frequency and secondary frequency excursion by solving two Lagrangian programming issues. Generally, inertial control is performed for frequency regulation by releasing the rotor kinetic energy, which causes a significant decrease in rotor speed. The greater the release of the rotor kinetic energy, the more active power is injected to the power system. When the rotor speed drops to its lower bound, the active power supply will be suspended, resulting in a secondary frequency drop. In addition, since the inertial control of the wind-storage coupling system is independent of frequency deviation, its frequency regulation capability may be insufficient. To deal with these issues, this paper proposes an FMPC to obtain the active power reference of the wind-storage coupling system by improving the frequency regulation performance in terms of second frequency drop, frequency nadir, and steady-state frequency deviation.

Active power reference received from frequency regulation requires appropriate allocation strategies to

ensure the inner parameter optimization of the wind-storage coupling system. Considering the number of the optimization objectives, active power allocation strategies have progressively evolved from single to multiple objectives. Various relevant control strategies have been proposed to perform active power allocation optimization with the single objective including mechanical load [18], rotor kinetic energy [19], or wind energy loss [20]. In light of the various guidelines created by grid standards and codes, two comprehensive active power allocation objectives are addressed in [21] to operate the WTGs at optimum points and minimize the wind tower torque. In [22], a dynamic active power allocation strategy is formulated for the wind farm to alleviate both the torque and rotor speed fluctuations. Furthermore, in [23], a hysteresis operator based active power allocation strategy is investigated for WTGs to simultaneously optimize the fatigue loads on the blade, shaft, and tower. In [24], an MPC is formulated in the active power allocation process to optimize the SOC of the BESS, shaft torque and rotor thrust fluctuations of the WTG. Recent attempts have considered different active power allocation strategies to mitigate the adverse impacts of the inner parameter deterioration on the WTG/BESS. However, in frequency regulation, the most popular active power allocation strategy, which optimizes the SOC and minimum rotor speed, could cause large drops of the SOC and rotor speed, potentially exceeding their lower limits. Consequently, the active power shortage can result in active power supply suspension, resulting in poor frequency response performance. To effectively use the frequency regulation resources of the wind-storage coupling system, an MMPC is proposed to raise the minimum rotor speed, minimize the pitch angle deviation and SOC deviation during active power allocation.

Previous studies employ decentralized strategies to accomplish active power allocation optimization. The essence of decentralized strategies is that the subsystem managers handle the optimization issue according to their mutually exchanged information, without the need for a centralized coordinator [25], [26]. However, the control communication delay, electromechanical transmission information conflict, and complicated control logic of subsystems in decentralized strategy can impair the active power allocation efficiency. In reality, large wind-storage coupling system usually has large amounts of output and control variables. With the expansion of wind-storage coupling system, the decentralized control techniques introduce heavy computation burdens. Take a wind-storage coupling system consisting of 800 WTGs and a BESS for example, the time consumption of the decentralized strategy in [25] amounts to more than 4 hours. On the other hand, in the wind-storage coupling system, the derived active power reference is distributed to the regulated objectives of the WTGs/BESS by optimizing the minimum rotor speed, pitch angle deviation and SOC deviation. Thus, active power allocation optimization is essentially a centralized problem. Consequently, a key challenge lies in transforming this centralized framework into a distributed one. In this paper, a distributed DAIA is proposed to realize the distributed framework conversion and efficient active power reference allocation during frequency regulation. Different from these decentralized control techniques, the proposed distributed DAIA combines the advantages of Lagrangian relaxation [27], [28] and multiplier approach [29], by decomposing the high dimensional optimization problem into low a dimensional optimization problem for the parallel computation.

Based on the above research issues, the motivation of this paper is to propose the DAMPC control for frequency regulation control and active power allocation of the wind-storage coupling system under severe step load conditions. The primary innovations can be outlined as follows.

1) In the top-level controller, FMPC is developed to generate the active power reference of the wind-storage coupling system through discretizing the grid frequency dynamic model and minimizing the frequency deviation. The frequency reference is calculated by considering the active power deviation and its integral, by the utilization of droop and inertial control, whereas the existing active power reference is determined only by using the inertial control. The proposed FMPC can provide high frequency regulation performance.

2) In the bottom-level controller, MMPC is designed to allocate the active power reference of the wind-storage coupling system to WTGs and BESS by raising the minimum rotor speed, minimizing the pitch angle deviation and SOC deviation. However, existing active power allocation methods typically consider at most two objectives, i.e., raising the minimum rotor speed and minimizing SOC deviation.

3) To solve the multi-objective allocation optimization problem with high efficiency, DAIA is proposed to allocate the active power reference of the wind-storage coupling system to WTGs and BESS by iteratively update the global and local active power control vectors with dual vectors. Since DAIA is a parallel computation technique and implemented through dimensional decomposition, the computational complexity between the WTGs/BESS and the wind-storage coupling system can be greatly reduced.

The rest of this paper is arranged as follows. The structure of the DAMPC strategy is presented in Section II. The top-level FMPC strategy is detailed in Section III, whereas the bottom-level MMPC strategy is described in Section IV. In Section V, detailed analysis

and verification of the FMPC and MMPC strategies are conducted to manifest the effectiveness of the proposed DAMPC strategy. Finally, the conclusion is drawn in Section VI.

II. Structure of the DAMPC Strategy

A. Topology Structure of the Wind-storage Coupling System

The investigated topology structure of the local power grid connected wind-storage coupling system is depicted in Fig. 1. The wind-storage coupling system G_4 is assumed to consist of 6 IEEE Type 3 WTGs and a centralized BESS. All 6 WTGs are equally distributed in two rows, and the BESS is integrated into the common bus through a DC/AC converter used for voltage conversion. The local power grid consists of 3 conventional generators (G_1–G_3), and a total of 11 buses (Bus1–Bus11) and 4 lines (Line1–Line4). The active power loads L_A, L_B, and L_C are located at Bus8, Bus9, and Bus10, separately.

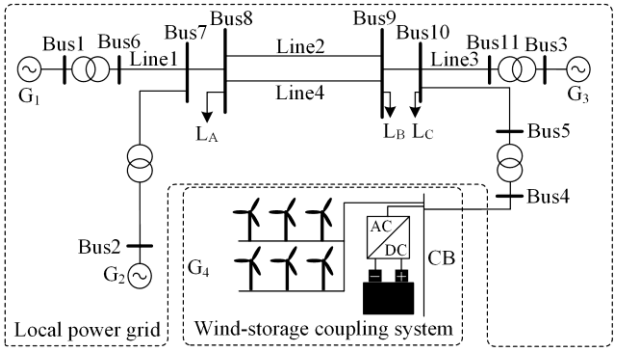

Fig. 1. Topology structure of local power grid-connected wind-storage coupling system.

B. Control Structure of the Proposed DAMPC Strategy

Figure 2 depicts the control structure of the proposed DAMPC strategy. The top-level controller is designed for the active power reference acquisition of the wind-storage coupling system and the bottom-level controller is designed for the active power reference allocation to the WTGs/BESS.

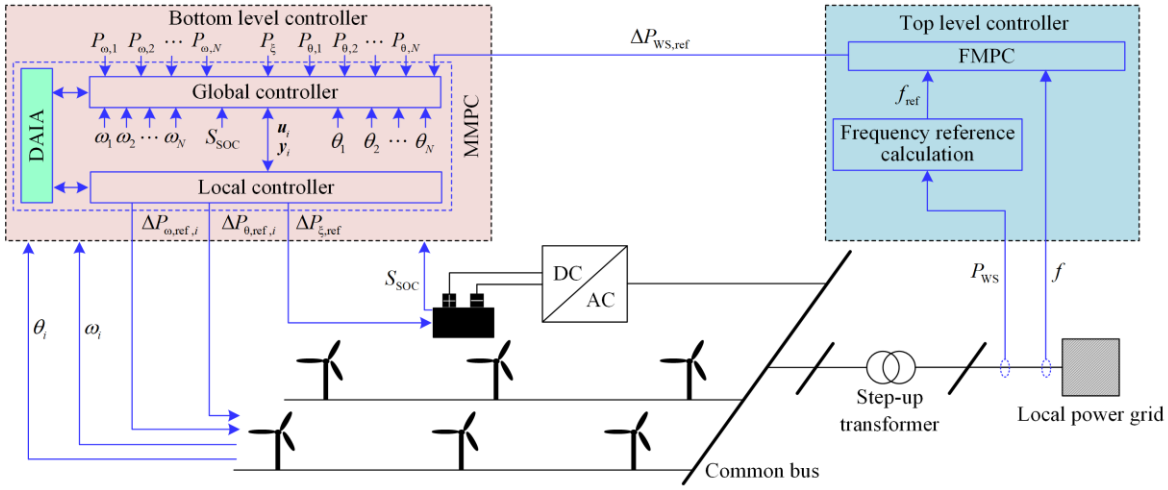

Fig. 2. Control structure of the proposed DAMPC strategy.

The top-level controller employs the FMPC strategy to obtain the active power reference by improving the frequency regulation performance. After measuring the frequency f of the local power grid and the active power P_{WS} of the wind-storage coupling system, the corresponding active power reference $\Delta P_{\mathrm{WS,ref}}$ is obtained by minimizing the frequency deviation, where the frequency reference f_{ref} takes the active power deviation and its integral into consideration. The derived active power reference is subsequently transmitted to the bottom-level controller.

The bottom-level controller, which consists of global and local controllers, employs the MMPC strategy to perform the active power allocation by raising the minimum rotor speed, while minimizing the pitch angle deviation and SOC deviation. After receiving the active power reference $\Delta P_{\mathrm{WS,ref}}$ and the initialization information (rotor speed, active power, pitch angle, and SOC) from the top-level controller, the proposed DAIA divides and assigns this reference to the WTGs and BESS. During the implementation of the proposed DAIA, the global controller is used to solve the augmented Lagrangian function of the wind-storage coupling system with the power equation constraints, while the local controller is utilized to solve the sub-augmented Lagrangian function of the WTGs/BESS with active power inequality constraints. During the entire DAIA optimization, the high dimension optimization problem of MMPC is transformed into low dimension global and local optimization issues solved in a parallel manner, exhibiting a high calculation efficiency.

III. TOP-LEVEL FMPC STRATEGY

In the proposed FMPC, the active power reference of the wind-storage coupling system is generated by minimizing the cost function of the frequency deviation, where the frequency reference is deduced using droop and inertial control. Since the frequency reference is finally formulated using the active power deviation and its integral, the proposed FMPC can improve the second frequency drop, frequency nadir, and steady-state frequency deviation.

When the power supply and load consumption are not equal, the actual frequency will deviate from its nominal value. From the relationship between the frequency and active power [30], the grid frequency dynamic model can be expressed by the first order linear differential equation, as:

$$\frac{2H_{\mathrm{G}}}{f_{\mathrm{N}}}\times\frac{\mathrm{d}f}{\mathrm{d}t}=P_{\mathrm{G}}+P_{\mathrm{WS}}-P_{\mathrm{L}}+D_{\mathrm{F}}P_{\mathrm{LN}}\left(1-\frac{f}{f_{\mathrm{N}}}\right) \tag{1}$$

If the grid frequency and output active power of the wind-storage coupling system are considered as output and control variables, respectively, then the grid frequency incremental prediction model is written as:

$$\Delta\dot{f}=-\frac{D_{\mathrm{F}}P_{\mathrm{LN}}}{2H_{\mathrm{G}}}\Delta f+\frac{f_{\mathrm{N}}}{2H_{\mathrm{G}}}\Delta P_{\mathrm{WS}}-\frac{f_{\mathrm{N}}\Delta P_{\mathrm{L}}}{2H_{\mathrm{G}}} \tag{2}$$

The cost function of the FMPC is defined as:

$$\min\ F_{\mathrm{F}}=\sum_{k=1}^{N_{\mathrm{T}}}\left[f(k)-f_{\mathrm{ref}}(k)\right]^2 \tag{3}$$

The utilization of inertia and droop control is beneficial in improving the dynamic and steady-state performance of the frequency response [31]. Thus, the frequency reference can be calculated by the active power deviation and its integral as:

$$\begin{aligned}f_{\mathrm{ref}}(k)=f_{\mathrm{N}}+K_{\mathrm{D}}\left[P_{\mathrm{G}}(k)-P_{\mathrm{L}}(k)+P_{\mathrm{WS}}(k)\right]/P_{\mathrm{LN}}+\\ K_{\mathrm{I}}\left[P_{\mathrm{G}}(k)-P_{\mathrm{L}}(k)+P_{\mathrm{WS}}(k)\right]/\left(sP_{\mathrm{LN}}\right)\end{aligned} \tag{4}$$

In practical applications, the output active power of the wind-storage coupling system satisfies the following constraint:

$$0\leqslant P_{\mathrm{WS},0}+\Delta P_{\mathrm{WS}}\leqslant P_{\mathrm{WS,max}} \tag{5}$$

The grid frequency incremental prediction model (2), cost function (3), frequency reference (4), and constraint (5) together form an optimization issue. Solving this problem yields the optimal ΔP_{WS}, which is then used as the active power reference $\Delta P_{\mathrm{WS,ref}}$ for the bottom-level controller.

IV. BOTTOM-LEVEL MMPC STRATEGY

In previous studies, the active power reference of the wind-storage coupling system is coordinated to optimize at most two objectives (raising minimum rotor speed and minimizing SOC deviation). In contrast, the proposed MMPC raises the minimum rotor speed, and minimizes the pitch angle deviation and SOC deviation during the active power reference allocation. Thus, the frequency regulation resources of the wind-storage coupling system can be effectively explored.

In the proposed MMPC, after receiving the active power reference $\Delta P_{\mathrm{WS,ref}}$ from FMPC, the bottom controller optimizes and allocates the active power reference $\Delta P_{\mathrm{WS,ref}}$ to the WTGs and BESS via DAIA. In this section, separate model predictive control strategies for the WTGs and BESS with different control objectives are built first, and the MMPC strategy is then established by combining these separate model predictive control strategies. Finally, the distributed DAIA is proposed to allocate the active power reference of the wind-storage coupling system to WTGs and BESS.

A. Rotor Speed Model Predictive Control

For WTG i, the rotor speed model predictive control regulates the output active power through the rotor speed to ensure the rotor speed regulating active power deviation $\Delta P_{\omega,i}$ to follow its reference $\Delta P_{\omega,\mathrm{ref},i}$. This model predictive control is applied to raise the minimum rotor speed of the WTG and avoid a secondary frequency droop.

The dynamic characteristic of the rotor can be described by the rotor motion equation [32]. By discretizing the rotor motion equation, the rotor speed incremental prediction model for the WTG i is written as:

$$\begin{cases}\Delta\dot{\boldsymbol{x}}_i=\boldsymbol{A}_i\Delta\boldsymbol{x}_i+\boldsymbol{B}_i\Delta\boldsymbol{u}_i+\boldsymbol{D}_i\\ \Delta\boldsymbol{y}_i=\boldsymbol{C}_i\Delta\boldsymbol{x}_i\end{cases} \tag{6}$$

with:

$$\begin{cases}\Delta\boldsymbol{x}_i=\left[\Delta\omega_i,\Delta P_{\omega,i}\right]^{\mathrm{T}}\\ \Delta\boldsymbol{u}_i=\left[\Delta P_{\omega,\mathrm{ref},i}\right]^{\mathrm{T}}\\ \Delta\boldsymbol{y}_i=\left[\Delta\omega_i,\Delta P_{\omega,i}\right]^{\mathrm{T}}\\ \boldsymbol{A}_i=\begin{bmatrix}\dfrac{P_{\mathrm{e0},i}-P_{\mathrm{m0},i}}{2H_{\mathrm{W}}\omega_{0,i}^2} & \dfrac{1}{2H_{\mathrm{W}}\omega_{0,i}}\\ 0 & \dfrac{-1}{\tau_\omega}\end{bmatrix}\\ \boldsymbol{B}_i=\begin{bmatrix}0 & \dfrac{-1}{\tau_\omega}\end{bmatrix}^{\mathrm{T}}\\ \boldsymbol{D}_i=\begin{bmatrix}\dfrac{P_{\mathrm{m0},i}-P_{\mathrm{e0},i}}{2H_{\mathrm{W}}\omega_{0,i}} & 0\end{bmatrix}^{\mathrm{T}}\\ \boldsymbol{C}_i=\begin{bmatrix}1 & 1\end{bmatrix}\end{cases} \tag{7}$$

The objective of raising the minimum rotor speed can be transformed into converging the rotor speed to the average rotor speed. Therefore, the cost function of the rotor speed model predictive control is written as:

$$F_{\omega}=\min\ \sum_{i=1}^{N_{\mathrm{g}}}\sum_{k=1}^{N_{\mathrm{B}}}\left\|\Delta\omega_i(k)-\frac{1}{N_g}\sum_{i=1}^{N_{\mathrm{g}}}\omega_i(k)\right\|^2 \tag{8}$$

subject to:

$$0\leqslant P_{\omega,0,i}+\Delta P_{\omega,\mathrm{ref},i}\leqslant P_{\mathrm{wt},i}^{\mathrm{rated}} \tag{9}$$

B. Pitch Angle Model Predictive Control

For WTG i, the pitch angle model predictive control governs the output active power via the pitch angle such that the pitch angle regulating active power deviation $\Delta P_{\theta,i}$ tracks its corresponding reference $\Delta P_{\theta,\mathrm{ref},i}$. The pitch angle model predictive control guarantees the minimum wind energy loss.

According to the approximate linearization technique [33], the pitch angle incremental prediction model for WTG i is expressed as:

$$\begin{cases}\Delta\dot{\boldsymbol{x}}'=\boldsymbol{A}_i'\Delta\boldsymbol{x}_i'+\boldsymbol{B}_i'\Delta\boldsymbol{u}_i'\\ \Delta\boldsymbol{y}_i'=\boldsymbol{C}_i'\Delta\boldsymbol{x}_i'\end{cases} \tag{10}$$

with:

$$\begin{cases}\Delta\boldsymbol{x}_i'=\begin{bmatrix}\Delta\theta_i & \Delta P_{m,i} & \Delta P_{\theta,i}\end{bmatrix}^{\mathrm{T}}\\ \Delta\boldsymbol{u}_i'=\begin{bmatrix}\Delta\theta_{\mathrm{ref},i} & \Delta P_{\theta,\mathrm{ref},i}\end{bmatrix}^{\mathrm{T}}\\ \Delta\boldsymbol{y}_i'=\begin{bmatrix}\Delta\theta_i & \Delta P_{\mathrm{m},i} & \Delta P_{\theta,i}\end{bmatrix}^{\mathrm{T}}\\ \boldsymbol{A}_i'=\begin{bmatrix}-\dfrac{1}{\tau_\theta} & 0 & 0\\ 0 & 0 & -\dfrac{1}{\tau_\theta}\\ 0 & \dfrac{1}{T} & \dfrac{1}{T}\end{bmatrix}\\ \boldsymbol{B}_i'=\begin{bmatrix}\dfrac{1}{\tau_\theta} & 0\\ \dfrac{k_0}{\tau_\theta} & 0\\ 0 & -\dfrac{1}{T_\theta}\end{bmatrix}\\ \boldsymbol{C}_i'=\begin{bmatrix}1 & 0 & 0\\ 0 & 1 & 0\\ 0 & 0 & 1\end{bmatrix}\end{cases} \tag{11}$$

The reserved active power can be achieved for frequency regulation through regulating the pitch angle. Considering the pitch angle is proportional to wind energy loss, the cost function of the pitch angle model predictive control is constructed as:

$$F_{\theta}=\min\ \sum_{i=1}^{N_{\mathrm{g}}}\sum_{k=1}^{N_{\mathrm{B}}}\left\|\Delta\theta_i(k)\right\|^2 \tag{12}$$

subject to:

$$0\leqslant P_{\theta,0,i}+\Delta P_{\theta,\mathrm{ref},i}\leqslant P_{\mathrm{wt},i}^{\mathrm{rated}} \tag{13}$$

C. SOC Model Predictive Control of BESS

For BESS, the SOC model predictive control manipulates the output active power through SOC so that the SOC regulating active power deviation ΔP_{ξ} approaches its corresponding reference $\Delta P_{\xi,\mathrm{ref}}$. The cost function that minimizes the gap between SOC and its desired reference indicates a superior SOC maintenance level.

Within each SOC sampling period T_{S}, considering the control block of the BESS and the open loop transfer function between the input and output variables [34], the SOC incremental prediction model is expressed as:

$$\begin{cases}\Delta\dot{\boldsymbol{x}}_{\mathrm{E}}=\boldsymbol{A}_{\mathrm{E}}\Delta\boldsymbol{x}_{\mathrm{E}}+\boldsymbol{B}_{\mathrm{E}}\Delta\boldsymbol{u}_{\mathrm{E}}\\ \Delta\boldsymbol{y}_{\mathrm{E}}=\boldsymbol{C}_{\mathrm{E}}\Delta\boldsymbol{x}_{\mathrm{E}}\end{cases} \tag{14}$$

with:

$$\begin{cases}\Delta\boldsymbol{x}_{\mathrm{E}}=\begin{bmatrix}\Delta S_{\mathrm{SOC}} & \Delta P_{\xi} & \Delta P_{\mathrm{int}}\end{bmatrix}^{\mathrm{T}}\\ \Delta\boldsymbol{u}_{\mathrm{E}}=\Delta P_{\xi,\mathrm{ref}}\\ \Delta\boldsymbol{y}_{\mathrm{E}}=\begin{bmatrix}\Delta S_{\mathrm{SOC}} & \Delta P_{\xi}\end{bmatrix}^{\mathrm{T}}\\ \boldsymbol{A}_{\mathrm{E}}=\begin{bmatrix}0 & -\dfrac{1}{C_{\xi,\max}} & 0\\ 0 & \dfrac{-1}{\tau_\xi} & 0\\ 0 & -1 & 0\end{bmatrix}\\ \boldsymbol{B}_{\mathrm{E}}=\begin{bmatrix}0 & \dfrac{1}{\tau_\xi} & 1\end{bmatrix}^{\mathrm{T}}\\ \boldsymbol{C}_{\mathrm{E}}=\begin{bmatrix}1 & 0 & 0\\ 0 & 1 & 0\end{bmatrix}\end{cases} \tag{15}$$

The cost function of the SOC model predictive control is formulated as:

$$F_{\mathrm{SOC}}=\min\sum_{k=1}^{N_{\mathrm{B}}}\left\|S_{\mathrm{SOC}}(k)-S_{\mathrm{SOC,ref}}(k)\right\|^2 \tag{16}$$

subject to:

$$0\leqslant P_{\xi,0}+\Delta P_{\xi,\mathrm{ref}}\leqslant P_{\xi,\max} \tag{17}$$

D. Proposed Multi-objective Model Predictive Control

The bottom controller has N_g numbers of WTGs to provide electromagnetic power by simultaneously adjusting rotor speeds and pitch angles, and a single BESS to provide energy storage active power by adjusting SOC.

Combining the rotor speed, pitch angle, and SOC incremental prediction models, the multi-objective incremental predictive control model for the wind-storage coupling system is described as:

$$\begin{cases} \Delta\dot{\boldsymbol{x}} = \boldsymbol{A}\Delta\boldsymbol{x} + \boldsymbol{B}\Delta\boldsymbol{u} + \boldsymbol{D} \\ \Delta\boldsymbol{y} = \boldsymbol{C}\Delta\boldsymbol{x} \end{cases} \tag{18}$$

with:

$$\begin{cases} \Delta\boldsymbol{x} = \left[\Delta x_1, \Delta x', \cdots, \Delta x_{\mathrm{N}}, \Delta x'_{\mathrm{N}}, \Delta x_{\mathrm{E}}\right]^{\mathrm{T}} \\ \Delta\boldsymbol{u} = \left[\Delta u_1, \Delta u'_1, \cdots, \Delta u_{\mathrm{N}}, \Delta u'_{\mathrm{N}}, \Delta u_{\mathrm{E}}\right]^{\mathrm{T}} \\ \Delta\boldsymbol{y} = \left[\Delta y_1, \Delta y'_1, \cdots, \Delta y_{\mathrm{N}}, \Delta y'_{\mathrm{N}}, \Delta y_{\mathrm{E}}\right]^{\mathrm{T}} \\ \boldsymbol{A} = \mathrm{Diag}\left[\boldsymbol{A}_1, \boldsymbol{A}'_1, \cdots, \boldsymbol{A}_{\mathrm{N}}, \boldsymbol{A}'_{\mathrm{N}}, \boldsymbol{A}_{\mathrm{E}}\right]^{\mathrm{T}} \\ \boldsymbol{B} = \mathrm{Diag}\left[\boldsymbol{B}_1, \boldsymbol{B}'_1, \cdots, \boldsymbol{B}_{\mathrm{N}}, \boldsymbol{B}'_{N}, \boldsymbol{B}_{\mathrm{E}}\right]^{\mathrm{T}} \\ \boldsymbol{C} = \mathrm{Diag}\left[\boldsymbol{C}_1, \boldsymbol{C}'_1 \ldots, \boldsymbol{C}_{\mathrm{N}}, \boldsymbol{C}'_{N}, \boldsymbol{C}_{\mathrm{E}}\right]^{\mathrm{T}} \\ \boldsymbol{D} = \mathrm{Diag}\left[\boldsymbol{D}_1, \boldsymbol{0} \ldots, \boldsymbol{D}_{\mathrm{N}}, \boldsymbol{0}, \boldsymbol{0}\right]^{\mathrm{T}} \end{cases} \tag{19}$$

By discretizing the state equation (19) with sampling time ΔT_{P}, the incremental discrete state equation is expressed as:

$$\begin{cases} \Delta\boldsymbol{x}(k+1) = \boldsymbol{G}\Delta\boldsymbol{x}(k) + \boldsymbol{H}\boldsymbol{u}(k) + \boldsymbol{D} \\ \Delta\boldsymbol{y}(k+1) = \boldsymbol{C}\Delta\boldsymbol{x}(k+1) \end{cases} \tag{20}$$

with:

$$\begin{cases} \boldsymbol{G} = \mathrm{e}^{\boldsymbol{A}\Delta T_{\mathrm{P}}} \\ \boldsymbol{H} = \int_0^{\Delta T_{\mathrm{P}}} \mathrm{e}^{\boldsymbol{A}\tau}\boldsymbol{B}\mathrm{d}\tau \end{cases} \tag{21}$$

Combining (8), (12) and (16), the integrated cost function is expressed as:

$$F_{\mathrm{C}} = F_{\omega} + F_{\theta} + F_{\mathrm{SOC}} = \min \sum_{i=1}^{N_{\mathrm{g}}}\sum_{k=1}^{N_{\mathrm{B}}}\left(\left\|\Delta\omega_i(k) - \frac{1}{N_{\mathrm{g}}}\sum_{i=1}^{N_{\mathrm{g}}}\omega_i(k)\right\|^2 + \left\|\Delta\theta_i(k)\right\|^2\right) + \sum_{k=1}^{N_{\mathrm{B}}}\left\|S_{\mathrm{SOC}}(k) - S_{\mathrm{SOC,ref}}(k)\right\|^2 \tag{22}$$

It should be noted that, in addition to satisfying the inequality constraints (9), (13), and (17), the integrated cost function needs to satisfy the following active power equation constraint:

$$\sum_{i=1}^{N_g}\Delta P_{\theta,\mathrm{ref},i} + \sum_{i=1}^{N_g}\Delta P_{\omega,\mathrm{ref},i} + \Delta P_{\xi,\mathrm{ref}} = \Delta P_{\mathrm{WS,ref}} \tag{23}$$

Since there is a considerable number of state equations related to the WTGs and BESS, the multi-objective model predictive control formed by (9), (13), (17), (22), and (23) suffers a high dimensional optimization challenge. However, DAIA can explore and simplify the solution procedure by dimensional decomposition and parallel calculation.

E. DAIA Solution for Active Power Allocation

In reality, a wind-storage coupling system is typically made up of hundreds or even thousands of WTGs. Thus, the predictive models and constraints become more complicated. If the conventional decentralized approach is applied, the computation burden increases significantly, potentially leading to the "curse of dimensionality". In order to solve this MMPC optimization problem more efficiently, the distributed DAIA is proposed to alternately and iteratively update the global and local control vectors with the dual control vector. In the proposed DAIA, the original optimization problem can be described as:

$$\min \sum_{i=1}^{N_g}\sum_{k=1}^{N_{\mathrm{B}}}\left[\left\|\Delta\omega_i(k) - \frac{1}{N_g}\sum_{i=1}^{N_g}\omega_i(k)\right\|^2 + \left\|\Delta\theta_i(k)\right\|^2\right] + \sum_{k=1}^{N_{\mathrm{B}}}\left\|S_{\mathrm{SOC}}(k) - S_{\mathrm{SOC,ref}}(k)\right\|^2 \tag{24}$$

Formula (24) is subject to $\boldsymbol{u} - \boldsymbol{U} = 0$, where $\boldsymbol{u}$ and $\boldsymbol{U}$ are the local control vectors and global control vectors, respectively.

The augmented Lagrangian function of the wind-storage coupling system in the global controller is expressed as:

$$\min \sum_{i=1}^{N_{\mathrm{g}}}\sum_{k=1}^{N_{\mathrm{B}}}\left[\left\|\Delta\omega_i(k) - \frac{1}{N_{\mathrm{g}}}\sum_{i=1}^{N_{\mathrm{g}}}\omega_i(k)\right\|^2 + \left\|\Delta\theta_i(k)\right\|^2 + \left\|S_{\mathrm{SOC},i}(k) - S_{\mathrm{SOC,ref},i}(k)\right\|^2\right] + \boldsymbol{y}^{\mathrm{T}}\left(\boldsymbol{u} - \boldsymbol{U}\right) + \frac{\gamma}{2}\left\|\boldsymbol{u} - \boldsymbol{U}\right\|_2^2 \tag{25}$$

where $\boldsymbol{y}$ is the dual vector; and γ is the penalty coefficient to magnify the gap between the local and the global control vectors.

The augmented Lagrangian function is separable over the components of the control vector. Thus, the sub-augmented Lagrangian function of WTG i and BESS in the local controller is expressed as:

$$\min \sum_{k=1}^{N_B} \left[\left\| \Delta\omega_i(k) - \frac{1}{N_g} \sum_{i=1}^{N_g} \omega_i(k) \right\|^2 + \left\| \Delta\theta_i(k) \right\|^2 + \frac{1}{N_g} \left\| S_{SOC}(k) - S_{SOC,ref}(k) \right\|^2 \right] + \boldsymbol{y}^T (\boldsymbol{u}_i - \boldsymbol{U}_i) + \frac{\gamma}{2} \left\| \boldsymbol{u}_i - \boldsymbol{U}_i \right\|_2^2 \quad (26)$$

By decomposing the augmented Lagrangian function of the global controller into the sub-augmented Lagrangian function of the local controller, the global and local control vectors can be updated iteratively.

Assuming the iteration index is τ, the specific procedures of DAIA are concluded as follows:

Step 1: Initialize the input variables. Set $\boldsymbol{u}$, $\boldsymbol{U}$ and $\boldsymbol{y}$ to 0 and the iteration index τ to 1, initialize the primal and dual thresholds δ_{pri}, δ_{dua}.

Step 2: Update the global control vector. Obtain the global control vector $\boldsymbol{U}$ by solving the augmented Lagrangian function with constraint:

$$\boldsymbol{U}(\tau+1) = \arg\min_{\boldsymbol{U}} \boldsymbol{y}^T(\tau)\left[\boldsymbol{u}(\tau) - \boldsymbol{U}\right] + \frac{\gamma}{2} \left\| \boldsymbol{u}(\tau) - \boldsymbol{U} \right\|_2^2 \quad (27)$$

subject to (23).

Step 3: Update the local control vector. Assign the component vector $\boldsymbol{U}_i$ in $\boldsymbol{U}$ to the corresponding WTG i and update its $\boldsymbol{u}_i$ by solving the sub-augmented Lagrangian function of the local controller:

$$\boldsymbol{u}_i(\tau+1) = \arg\min_{u_i} \left\| \Delta\omega_i(k) - \frac{1}{N_g} \sum_{i=1}^{N_g} \omega_i(k) \right\|^2 + \left\| \Delta\theta_i(k) \right\|^2 + \frac{1}{N_g} \left\| S_{SOC}(k) - S_{SOC,ref}(k) \right\|^2 + \boldsymbol{y}^T(\tau)\left(\boldsymbol{u}_i - \boldsymbol{U}_i(\tau+1)\right) + \frac{\gamma}{2} \left\| \boldsymbol{u}_i - \boldsymbol{U}_i(\tau+1) \right\|_2^2 \quad (28)$$

Equation (28) is subject to (9), (13) and (17).

Step 4: Renew the dual vector. Update the dual control vector as:

$$\boldsymbol{y}_i(\tau+1) = \boldsymbol{y}_i(\tau) + \gamma\left[\boldsymbol{u}_i(\tau+1) - \boldsymbol{U}_i(\tau+1)\right] \quad (29)$$

Step 5: Check the convergence. Calculate and check if the primary residual $p_i(\tau)$ and dual residual $d_i(\tau)$ are within their predefined thresholds, i.e.:

$$\begin{cases} p_i(\tau) = \left\| \boldsymbol{u}(\tau) - \boldsymbol{U}(\tau) \right\|_2^2 \leqslant \delta_{pri} \\ d_i(\tau) = \left\| \boldsymbol{u}(\tau) - \boldsymbol{U}(\tau-1) \right\|_2^2 \leqslant \delta_{dua} \end{cases} \quad (30)$$

Once satisfied, terminate the iteration and output the results. Otherwise, let $\tau = \tau + 1$ and repeat Steps 2–4.

F. Frequency Response Model of the Proposed DAMPC Strategy

Based on (2), (7), (11) and (14), the frequency response model of the proposed DAMPC strategy can be seen in Fig. 3.

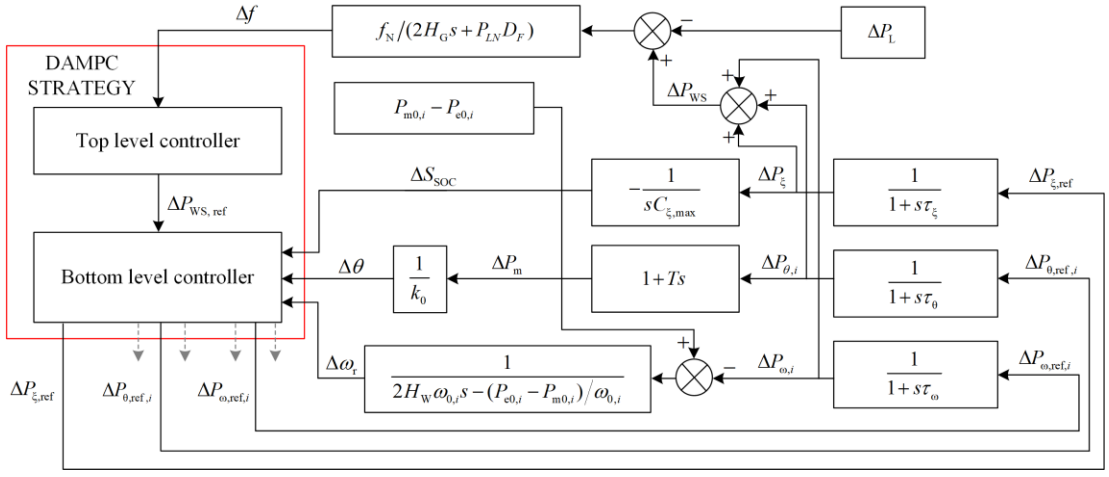

Fig. 3. Frequency response model of the proposed DAMPC strategy.

V. Case Study

A. System Description

In order to corroborate the effectiveness of the proposed DAMPC strategy, a local grid-connected wind-storage coupling system is simulated in MATLAB R2016b/Simulink using a personal laptop with the Intel i5 8250U 4-Core Processor. The key configuration parameters are set as following: solver type – variable-step; solver – Gurobi optimization solver; relative tolerance -2×10^{-5}; start time – 0 s; and stop time –11 s. The performance is tested and compared during a 30 MW active power increase at the local power grid. The main electrical equipment and control parameters are provided in Tables I and II, respectively.

In Table II, according to [8]–[10], there is a 0.1 s to 0.18 s time delay for the phase-locked loop to obtain the frequency information. Consequently, the grid frequency sampling period is set to 0.12 s. The top level FMPC transmits the active power reference to the bottom level MMPC, which involves three control objectives, i.e., rotor speed, pitch angle, and SOC. The rotor speed

sampling period, the pitch angle sampling period, and the SOC sampling period are all set to 0.04 s (0.12/3 s). In addition, the control/prediction time domains of both the top level FMPC controller and the bottom level MMPC controller are adjusted to 3 to achieve a balance between simulation time and accuracy.

TABLE I
ELECTRICAL EQUIPMENT PARAMETERS

	Parameters	Symbol	Value	Unit
Local power grid	Rated frequency	f_N	50	Hz
	Grid inertia constant	H_G	8520	$kg \cdot m^2$
	Grid frequency damping factor	D_F	4000	$kg \cdot m^2$
	Nominal active power of conventional generator	$P_{G1}/P_{G2}/P_{G3}$	100	MW
	Active power load	$P_{LA}/P_{LB}/P_{LC}$	117/35/97.5	MW
Wind-storage coupling system	Nominal active power of WTG	P_{WTG}	10	MW
	Time delay of pitch angle regulation	τ_θ	0.1	s
	WTG rotation inertia constant	H_W	2180	$kg \cdot m^2$
	Primary term coefficient of pitch angle	k_0	3	
	Maximum charge/discharge power of BESS	$P_{\xi,max}$	5	MW
	Time delay of active power regulated by BESS	τ_ξ	0.1	s
	Maximum SOC of BESS	$S_{SOC,max}$	0.9	
	Maximum charge/discharge capacity of BESS	$C_{\xi,max}$	0.25	MWh
	Minimum SOC of BESS	$S_{SOC,min}$	0.1	
	SOC reference of BESS	$S_{SOC,ref}$	0.8	

TABLE II
CONTROL PARAMETERS

Top-level FMPC controller		Bottom-level MMPC controller			
Grid frequency sampling period T_F (s)	0.12	Rotor speed sampling period T_R (s)	0.04	Primal threshold	10^{-10}
Control/prediction time domain N_T	3	Pitch angle sampling period T_θ (s)	0.04	Dual threshold	10^{-10}
Droop coefficient K_D	0.3	SOC sampling period T_S (s)	0.04	Penalty coefficient γ	10^7
Inertia coefficient K_I	0.06	Control/Prediction time domain N_B	3		

B. Comparison Control Strategies

In this paper, four other controls are performed sequentially for comparisons to validate the rationality and universality of the proposed DAMPC strategy: 1) Scheme 1 is the proposed DAMPC strategy; 2) Scheme 2 uses the multi-objective active power allocation strategy in Section IV, and the active power of the wind-storage coupling system is determined according to adaptive gain frequency control [8]; 3) Scheme 3 allocates equally the active power of the wind-storage coupling system to the WTGs and BESS by regulating the rotor speed, pitch angle and SOC, while the total active power of the wind-storage coupling system is excavated by four-stage transient frequency control [9]; 4) Scheme 4 is the two objective active power allocation control where the minimum rotor speed and SOC are optimized together by model predictive control, and the overall active power of the wind-storage coupling system is exploited by hierarchical coordinated inertia control [10]; and 5) Scheme 5 is the DAMPC strategy, where the multi-objective allocation optimization problem is solved with the additive increase multiplicative decrease algorithm [25].

The frequency regulation and active power allocation controls under Schemes 1–4 are compared in Table III.

TABLE III
CONTROL COMPARISONS OF FREQUENCY REGULATION AND ACTIVE POWER ALLOCATION

Control objective	Scheme 1	Scheme 2	Scheme 3	Scheme 4
Wind-storage coupling system	Grid frequency model predictive control	Adaptive gain frequency control	Four-stage transient frequency control	Hierarchical coordinated inertia control
WTGs/BESS	Multi-objective model predictive control	Multi-objective model predictive control	Equal active power allocation control	Two objective model predictive control

Because the performance of the proposed Scheme 1 is inevitably affected by the wind penetration rate, three scenarios are performed to evaluate the impact of wind penetration rate variation on the frequency deviation.

Scenario 1: For the low wind penetration scenario, the wind penetration rate is set to 25%.

Scenario 2: For the medium wind penetration scenario, the wind penetration rate is set to 37%.

Scenario 3: For the high wind penetration scenario, the wind penetration rate is set to 48%.

C. FMPC Analysis and Verification

Since a step load represents an extreme condition for validating test schemes, load A is assumed to increase abruptly by 30 MW at 1 s, causing a low frequency event in the power system. Figure 4 and Table IV compare the second frequency drops and frequency deviations with Schemes 1-4. According to Fig 4, Scheme 3 results in the most severe second frequency drop because of the available time-dependent active power reference during the rotor speed recovery period. Scheme 4 has a relative lower second frequency drop than Scheme 3 since its active power reference is determined by simultaneously optimizing primary and secondary frequency deviations. Compared with Schemes 3 and 4, Scheme 2 has a lower second frequency drop, due to its output active power gain being proportional to rotor kinetic energy and thus avoiding excessive deceleration in the rotor recovery stage. However, with the frequency reference determined by the active power deviation and its integral, Scheme 1 can thoroughly eliminate the second frequency drop with the cost function of minimizing frequency deviation. Therefore, the total active power reference of the wind-storage coupling system with Scheme 1 outperforms those of other schemes on the second frequency drop performance.

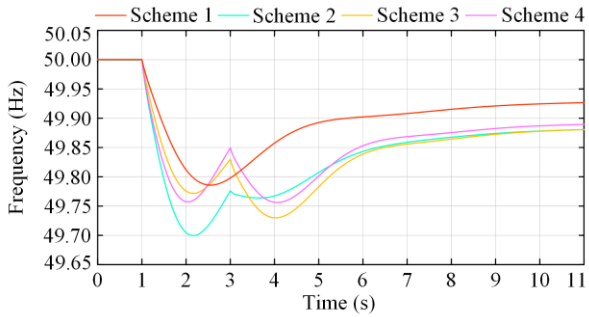

Fig. 4. Second frequency drop comparison with Schemes 1–4.

TABLE IV
COMPARISONS WITH SCHEMES 1–4 OVER VARIOUS FREQUENCY DEVIATIONS

	Scheme 1	Scheme 2	Scheme 3	Scheme 4
Steady state frequency deviation (Hz)	0.075	0.121	0.121	0.112
Maximum frequency deviation (Hz)	0.214	0.300	0.270	0.244

Table IV compares the steady-state frequency deviation and maximum frequency deviation under Schemes 1–4. As can be seen, Scheme 1 is capable of minimizing both the steady-state and maximum frequency deviations. In contrast to Scheme 2, Scheme 1 decreases the steady-state frequency deviation by 0.046 Hz and the maximum frequency deviation by 28.667%. Compared to Scheme 3, Scheme 1 reduces the steady-state and maximum frequency deviations by 0.046 Hz and 20.74%, respectively, whereas they are reduced by 0.037 Hz and 12.295%, respective, when compared to Scheme 4. The steady-state and maximum frequency deviations are primarily dependent on the active power output, while Fig. 5 shows the active power output of the wind-storage coupling system under Schemes 1–4. According to Fig. 5, the larger the steady-state and maximum frequency deviations, the smaller the active power output. In terms of active power output, Scheme 1 is the largest, followed by Schemes 3 and 4, with Scheme 2 having the smallest. Therefore, Scheme 1 can obtain the largest active power reference resulting in the smallest frequency deviation.

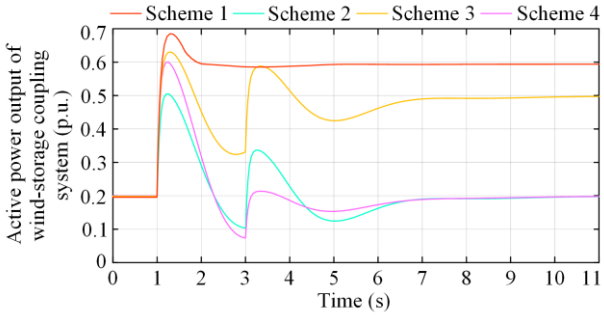

Fig. 5. Active power output of the wind-storage coupling system with Schemes 1–4.

The frequency nadirs with Schemes 1–4 under the three wind penetration rates are shown in Fig. 6. With the same control implementation, the higher the wind penetra-tion rate, the smaller the frequency nadir under the step load disturbance. This is because high wind pen-etration severely impairs the overall inertia of the power grid. On the other hand, regardless of the wind penetration rate, Scheme 1 consistently yields the highest frequency nadir when the wind penetra-tion rate is fixed. Thus, Scheme 1 effectively im-proves the frequency nadir under all wind penetration conditions.

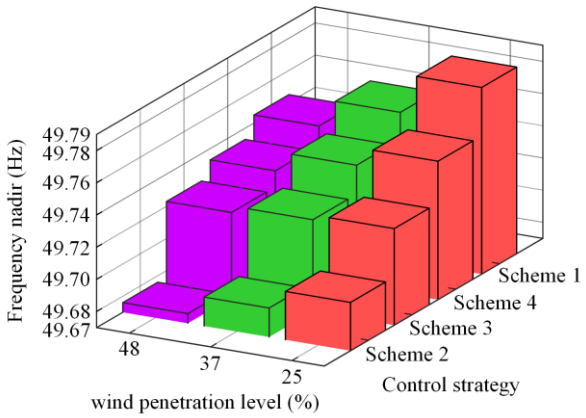

Fig. 6. Frequency nadir with Schemes 1–4 under three wind penetration levels.

D. MMPC Analysis and Verification

In the MMPC strategy, the initial values of WTGs and BESS are the premise condition for the implementation of the active power allocation. The initial pitch angles, wind speeds, and rotor speeds of the WTGs are shown in Fig. 7. Specifically, the initial pitch angles for the six WTGs are 17.5, 14.75, 11.25, 9.00, 6.25, and 4 degrees, while the wind speeds of the six WTGs are 15.5, 14.1, 13.0, 12.1, 11.2, and 10.5 m/s, respectively. Based on the initial pitch angle and wind speed information, the initial rotor speeds can be computed according to the mechanical power curve, i.e., 1.186, 1.150, 1.136, 1.100, 1.062, and 1.027 rad/s, respectively. The initial value of SOC is set to 0.8. Since Schemes 1, 3, and 4 have smaller maximum frequency deviations compared with Scheme 2, these three schemes are chosen to verify the rotor speed, pitch angle and SOC performance of the proposed MMPC.

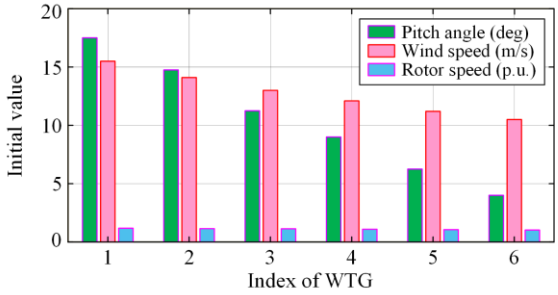

Fig. 7. Initial pitch angle, wind speed and rotor speed of WTG.

1) Rotor Speed Verification

Figures 8–10 present the rotor speeds with Schemes 1, 3 and 4, respectively. As can be seen, before the step load disturbance, a consistent rotor speed can be observed with different schemes if the indices of the WTGs are identical. After the step load appears, the rotor speeds of Schemes 1, 3 and 4 first decrease and then increase because the rotors release the stored kinetic energy to compensate for the active power shortage for frequency regulation. Compared with Scheme 3, Schemes 1 and 4 with active power allocation optimized by model predictive control raise the minimum rotor speeds significantly. In comparison with Scheme 4, the proposed Scheme 1 further improves the minimum rotor speed, due to its allocation of the whole active power by optimizing the minimum rotor speed, pitch angle and SOC, whereas Scheme 4 allocates the active power of the wind-storage coupling system only by optimizing the minimum rotor speed and SOC. Since Scheme 1 has more power supply resources than Scheme 4, its minimum rotor speed drops to a relative higher value than that of Scheme 4, i.e., the minimum rotor speed reaching 1.088 rad/s in Scheme 1 compared to 1.058 rad/s in Scheme 4. Thus, Scheme 1 achieves a better performance in raising minimum rotor speed during the active power allocation.

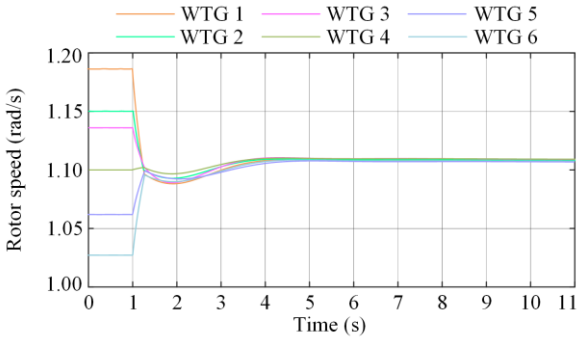

Fig. 8. Rotor speed with Scheme 1.

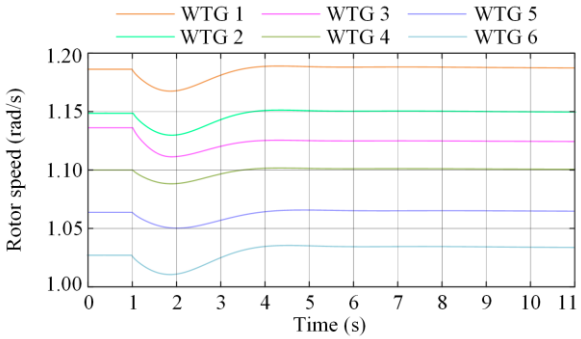

Fig. 9. Rotor speed with Scheme 3.

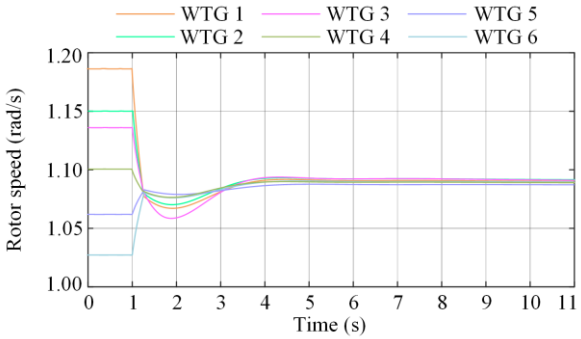

Fig. 10. Rotor speed with Scheme 4.

2) Pitch Angle Verification

Figures 11–13 provide the pitch angles under Schemes 1, 3 and 4. As can be seen, since Scheme 3 allocates equally the active power to regulate the rotor speed, pitch angle, and SOC, the pitch angles of different WTGs become dispersed following the step load disturbance. The total pitch angle deviation of all the WTGs under Scheme 3 is the largest, indicating the largest wind power loss. Although both Schemes 1 and 4 optimize the active power allocation with model predictive control, the pitch angles of WTGs converge to different fixed values of 0.6 degree under Scheme 1 and 5 degrees under Scheme 4. The difference is caused by the different active power allocation control objectives, i.e., Scheme 4 focuses only on two objectives of minimum rotor speed and SOC, whereas Scheme 1 considers the three objectives of minimum rotor speed,

pitch angle and SOC. Thus, Scheme 1 achieves a better performance on minimizing the pitch angle deviation.

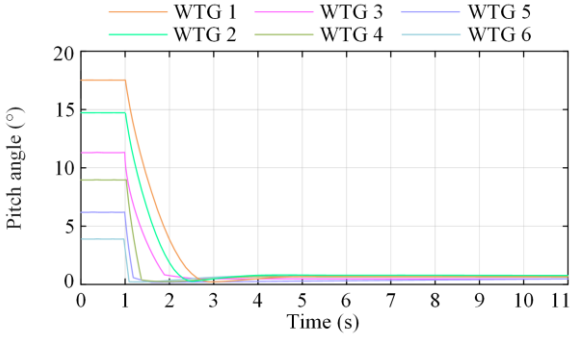

Fig. 11. Pitch angle with Scheme 1.

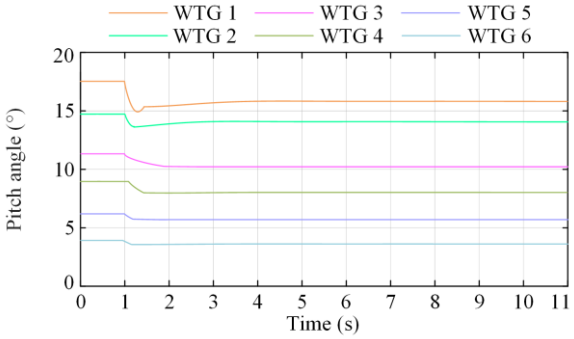

Fig. 12. Pitch angle with Scheme 3.

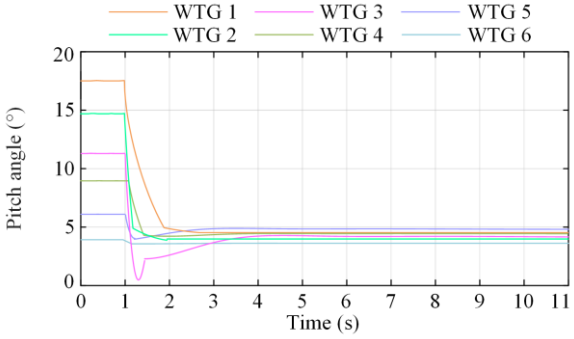

Fig. 13. Pitch angle with Scheme 4.

3) SOC Verification

Figure 14 portrays the SOC curves under Schemes 1, 3 and 4. As can be seen, after the step load disturbance at 1 s, the SOC curves with the three comparative schemes display distinguished declining trajectories. Specifically, the SOC curves under Schemes 4 and 1 decline with approximate exponential forms, whereas it displays a linear decrease under Scheme 3. The variations in the SOC curves can be attributed to whether active power allocation is based on model predictive control. During the post period of Fig. 14, the SOC level under Schemes 1 is better than those under Schemes 3 and 4. For example, at around 11 s, the SOC level under Scheme 1 is 21.883% and 8.333% higher than those under Schemes 3 and 4, respectively. This is because Scheme 1 optimizes the rotor speed, pitch angle, and SOC to regulate and match the active power required by the wind-storage coupling system, whereas Scheme 4 only optimizes the rotor speed and SOC to regulate active power supply while Scheme 3 equally deploys the total active power to regulate the rotor speed, pitch angle, and SOC without optimization. Thus, Scheme 1 is capable of reducing the SOC deviation more effectively than other schemes during the active power allocation.

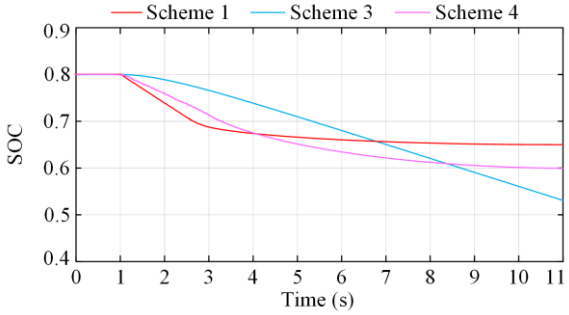

Fig. 14. SOC curves with Schemes 1, 3 and 4.

4) DAIA Solution Efficiency Verification

To further show the convergence performance of Scheme 1, tests are carried out with 16 WTGs. For simplicity, the local control variables u_{1-2} and their corresponding global control variables U_{1-2} are considered as the representative variables. Figures 15–16 compare the convergence properties between Schemes 1 and 5 [25]. It is seen that Scheme 1 displays better convergence performance than Scheme 5. The local control variables u_{1-2} and their corresponding global control variables U_{1-2} of Scheme 1 converge to the same value after iteration index 19. In contrast, Scheme 5 converges to the same value of Scheme 1 after iteration index 22.

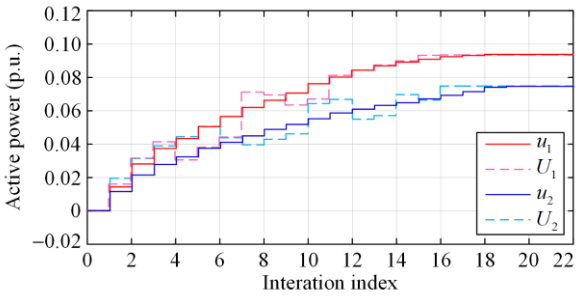

Fig. 15. Convergence performance with Schemes 1.

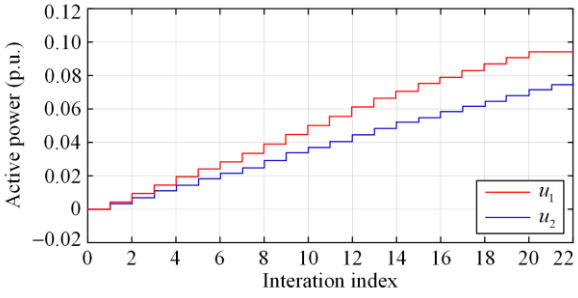

Fig. 16. Convergence performance with Schemes 5.

To check the solution efficiency of Scheme 1, Table V compares the solution times under Scheme 1 and 5, in which the solution times with 6, 16, 100, and 200 WTGs are calculated for verification. The larger the solution time, the lower the computational efficiency during the simulation. When the number of WTGs is 6, the computational efficiency with Scheme 1 is improved by 6.90% compared to Scheme 5, whereas the improvement rises to 71.43% when the number of WTGs reaches 200. This is because DAIA is an efficient parallel computation methodology and behaves more prominent in high dimensional decomposition and calculation. Consequently, the computational efficiency gains with Scheme 1 become more pronounced as the number of WTGs increases.

TABLE V
COMPARISON OF SOLUTION TIME WITH SCHEME 1 AND SCHEME 5

Scheme		6WTGs	16WTGs	100WTGs	200WTGs
Scheme 5		0.0754s	0.2029s	7.1439s	61.2399s
Scheme 1	Global controller	0.0027s	0.0047s	0.0633 s	0.4323 s
	Local controller	0.0051s	0.0051s	0.0051 s	0.0051 s
	Iteration times	9	19	34	40
	Total solution time of global controller	0.0243s	0.0893s	2.1522s	17.292s
	Total solution time	0.0702s	0.1862s	2.3256s	17.496s
Improved computation efficiency with Scheme 1		6.90%	8.23%	67.45%	71.43%

E. Discussion

The frequency reference formulated in the proposed FMPC strategy uses two key coefficients: droop coefficient K_D and inertia coefficient K_I. To assess the sensitivity of the proposed FMPC strategy to each coefficient in the frequency reference, variations are applied to the other coefficient while keeping one key coefficient constant. The impact of the droop coefficient K_D on frequency regulation performance is evaluated by three cases in scenario 1, i.e., Scenario 1-case 1: $K_D = 0.3$, $K_I = 0.06$; Scenario 1-case 2: $K_D = 0.2$, $K_I = 0.06$; and Scenario 1-case 3: $K_D = 0.1$, $K_I = 0.06$. On the other hand, the impact of the inertia coefficient K_I on frequency regulation performance is evaluated by three cases in scenario 2, i.e., Scenario 2-case 1: $K_D = 0.1$, $K_I = 0.06$; Scenario 2-case 2: $K_D = 0.1$, $K_I = 0.08$; and Scenario 2-case 3: $K_D = 0.1$, $K_I = 0.1$. Taking the step load increase in Section V C as an example, the frequency responses in the FMPC strategy with different frequency reference are shown in Fig. 17.

The black line represents the FMPC strategy with constant frequency reference (50 Hz), while the colored solid and colored dashed lines represent the influences of the droop coefficient and inertia coefficient on the grid frequency, respectively. As can be seen from Fig. 17, along with the increasing proportion of droop coefficient, the proposed FMPC strategy achieves a lower maximum frequency deviation and improve it more effectively than that with constant frequency reference. In addition, with the increasing inertia coefficient, the proposed FMPC strategy realizes a lower second frequency drop. Under steady state, the proposed FMPC strategy also achieves better frequency support performance than that with constant frequency reference. Therefore, under different coefficient scenarios, the proposed FMPC strategy achieves excellent frequency regulation performance.

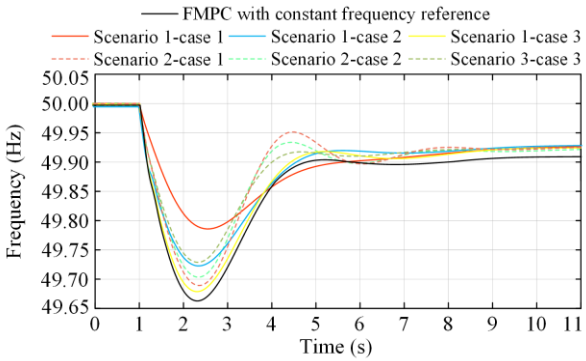

Fig. 17. Frequency response of FMPC strategy with different frequency reference.

VI. CONCLUSION

To realize frequency regulation control and active power allocation in wind-storage coupling systems, this paper proposes a two-level DAMPC strategy, which includes a top-level FMPC and a bottom-level MMPC. The performance of the proposed DAMPC strategy is verified through extensive simulations. The conclusions are drawn as follows.

1) To improve frequency regulation performance, the top-level FMPC is established to determine the active power reference of the wind-storage coupling system. The frequency reference of the FMPC is calculated by the active power deviation and its integral. Compared with the existing frequency regulation control methods, the steady-state frequency deviation and maximum frequency deviation of the FMPC are reduced by

20.08% and 56.62%, respectively, while the second frequency drop can be completely eliminated.

2) To raise the minimum rotor speed, minimize the pitch angle deviation and SOC deviation, the active power reference of the wind-storage coupling system is assigned to the WTGs and BESS through the bottom-level MMPC. The wind-storage coupling system with MMPC has the minimum rotor speed of 1.088 rad/s, the minimum pitch angle deviation of 0.6°, and the minimum SOC deviation, which are superior to other active power allocation control methods.

3) In order to enhance the solution efficiency of active power allocation, DAIA is proposed to alternatively and iteratively solve the multi-objective optimization problem. With the proposed DAIA, the solution efficiency is improved by at least 6.9% compared to existing decentralized algorithms.

Since the rotor speed variation, pitch angle variation, and SOC variation yield different levels of active power, MMPC with different weighting coefficients will be explored in future work.

ACKNOWLEDGMENT

Not applicable.

AUTHORS' CONTRIBUTIONS

Zhenhua Cai: conceptualization, methodology, software, visualization, and writing-original draft. Xubin Liu: conceptualization, methodology, writing-review, and supervision. Canbing Li: methodology and editing. Nengling Tai: writing-review and editing. Wentao Huang: supervision and revision. Sheng Huang: conceptualization and review. Juan Wei: review and editing. All authors read and approved the final manuscript.

FUNDING

This work is carried out without the support of any funding agency.

AVAILABILITY OF DATA AND MATERIALS

Not applicable.

DECLARATIONS

Competing interests: The authors declare that they have no known competing financial interests or personal relationships that could have appeared to influence the work reported in this article.

AUTHORS' INFORMATION

Zhenhua Cai received the M.S. degree in electrical engineering from Hunan University, Changsha, China in 2013, He is currently working towards the Ph.D. degree in electrical engineering from Hunan University. His present research interests involve wind power modelling and control, power system economic operation and renewable energy generation.

Xubin Liu received the Ph.D. degree in electrical engineering from Hunan University, Changsha, China, in 2019. From 2019 to 2021, he was a postdoctoral researcher with the School of Electrical and Electronic Engineering, Huazhong University of Science and Technology, Wuhan, China. He is currently an associate professor with the School of Automation, Central South University, Changsha. His research interests include power system stability analysis and control, active frequency and voltage support technology, power-electronic power network model and control, fault analysis and protection control, renewable energy integrated control, and energy management system of smart grid.

Canbing Li received the B.E. and Ph.D. degrees in electrical engineering from Tsinghua University, Beijing, China, in 2001 and 2006, respectively. He is currently associated with the School of Electronic Information and Electrical Engineering, Shanghai Jiao Tong University. His present research interests include power system economic dispatch, smart grid fault analysis and renewable energy generation and control.

Nengling Tai received the B.E. and Ph.D. degrees in electrical engineering from Huazhong University of Science and Technology, Wuhan, China, in 1994, and 2000, respectively. He is presently a professor with the Department of Power Electrical Engineering, shanghai Jiao Tong University, Shanghai, China. His research interests involve the HVDC transmission system and smart grid.

Wentao Huang received the Ph.D. degree in electrical engineering from Shanghai Jiao Tong University, Shanghai, China, in 2015. He is currently an associate professor with the Department of Power Electrical Engineering, Shanghai Jiao Tong University. His research interests involve protection and control of active distribution systems, microgrids, smart grid, and renewable energy.

Sheng Huang received the M.S. and the Ph.D. degrees from the College of Electrical and Information Engineering, Hunan University, Changsha, China, in 2012 and 2016, respectively. He is currently an associate professor in Hunan University, Changsha, China. He is

also a postdoc in the Center for Electric Power and Energy, technical University of Denmark, Kongens Lyngby, denmark. His research interests include renewable energy generation, operation and control.

Juan Wei received the B.S. and M.S. degrees in electrical engineering from North China Electric Power University, Beijing, China, in 2011 and 2014, respectively. She is currently a research fellow in Hunan University, Changsha, China. She was a visiting student with the Department of Electrical Engineering, Technical University of Denmark, Kongens Lyngby, Denmark. Her research interests involve renewable energy generation modelling and control and power system economic and secure operation.

REFERENCES

[1] M. A. A. Rani, M. Chakkarapani, and C. Nagamani *et al*., "An improved angular Stator flux frequency computation method for robust MPPT operation of DFIG under unbalanced grid voltage," *IEEE Transactions on Industry Applications*, vol. 59, no. 1, pp. 1162-1174, Jan. 2023.

[2] Y. Zhou, D. Zhu, and J. Hu *et al*., "Magnitude-phase characteristics analysis of inertia for DFIG-based wind turbines, *IEEE Transactions on Power Electronics*," vol. 39, no. 10, pp. 12336-12348, Oct. 2024.

[3] N. K. Roy, S. Islam, and A. K. Podder *et al*., "Virtual inertia support in power systems for high penetration of renewables—overview of categorization, comparison, and evaluation of control techniques," *IEEE Access*, vol. 10, pp. 129190-129216, Dec. 2022.

[4] J. -S. Kim, Y. -J. Kim, and O. Gomis-Bellmunt, "Optimal frequency regulation of multi-terminal HVDC-linked grids with deloaded offshore wind farms control," *IEEE Transactions on Sustainable Energy*, vol. 15, no. 1, pp. 290-303, Jan. 2024.

[5] L. Miao, J. Wen, and H. Xie *et al.*, "Coordinated control strategy of wind turbine generator and energy storage equipment for frequency support," *IEEE Transactions on Industry Applications*, vol. 51, no. 4, pp. 2732-2742, Jul. 2015.

[6] Y. Li, W. Li, and D. Yang *et al*., "Droop coefficient design of wind turbine considering rotor speed constraints," *IEEE Transactions on Sustainable Energy*, vol. 15, no. 3, pp. 2130-2133, Jul. 2024.

[7] Y. Xiong, W. Yao, and Z. Shi *et al*., "Adaptive dual droop control of MTDC integrated offshore wind farms for fast frequency support," *IEEE Transactions on Power Systems*, vol. 38, no. 3, pp. 2525-2538, May 2023.

[8] J. Lee, G. Jang, and E. Muljadi *et al*., "Stable short-term frequency support using adaptive gains for a DFIG-based wind power plant," *IEEE Transactions on Energy Conversion*, vol. 31, no. 3, pp. 1068-1079, Sept. 2016.

[9] D. Yang, J. Kim, and Y. C. Kang *et al*., "Temporary frequency support of a dfig for high wind power penetration," *IEEE Transactions on Power Systems*, vol. 33, no. 3, pp. 3428-3437, May 2018.

[10] W. Bao, Q. Wu, and L. Ding *et al*., "A hierarchical inertial control scheme for multiple wind farms with BESSs based on ADMM," *IEEE Transactions on Sustainable Energy*, vol. 12, no. 2, pp. 751-760, Apr. 2021.

[11] H. Wang and Z. Li, "Multi-area load frequency control in power system integrated with wind farms using fuzzy generalized predictive control method," *IEEE Transactions on Reliability*, vol. 72, no. 2, pp. 737-747, Jun. 2023.

[12] Y. Tang, P. Yang, and Y. Yang *et al*., "Fuzzy adaptive frequency support control strategy for wind turbines with improved rotor speed recovery," *IEEE Transactions on Sustainable Energy*, vol. 15, no. 2, pp. 1351-1364, Apr. 2024.

[13] X. Lyu, Y. Jia, and Z. Xu, "A novel control strategy for wind farm active power regulation considering wake interaction," *IEEE Transactions on Sustainable Energy*, vol. 11, no. 2, pp. 618-628, Apr. 2020.

[14] L. Xiong, S. Yang, and S. Huang *et al*., "Optimal allocation of energy storage system in DFIG wind farms for frequency support considering wake effect," *IEEE Transactions on Power Systems*, vol. 37, no. 3, pp. 2097-2112, May 2022.

[15] D. Cirio, F. Conte, and B. Gabriele *et al*., "Fast frequency regulation from a wind farm-BESS unit by model predictive control: method and hardware-in-the-loop validation," *IEEE Transactions on Sustainable Energy*, vol. 14, no. 4, pp. 2049-2061, Oct. 2023.

[16] W. Bao, Q. Wu, and L. Ding *et al*., "Synthetic inertial control of wind farm with BESS based on model predictive control," *IET Renewable Power Generation*, vol. 14, no. 13, pp. 2447-2455, 2020.

[17] N. Sockeel, J. Gafford, and B. Papari, "Virtual inertia emulator-based model predictive control for grid frequency regulation considering high penetration of inverter-based energy storage system," *IEEE Transactions on Sustainable Energy*, vol. 11, no. 4, pp. 2932-2939, Oct. 2020.

[18] S. Vedrana, J. Mate, and B. Mato, "Wind turbine power references in coordinated control of wind farms," *AUTOMATIKA*, vol. 52, no. 2, pp. 82-94, 2011.

[19] Y. Li, Z. Xu, and K. Meng, "Optimal power sharing control of wind turbines," *IEEE Transactions on Power Systems*, vol. 32, no. 1, pp. 824-825, Jan. 2017.

[20] H. Wang, Z. Chen, and Q. Jiang, "Optimal control method for wind farm to support temporary primary frequency control with minimised wind energy cost," *IET Renewable Power Generation*, vol. 9, no. 4, pp. 350-359, 2015.

[21] F. M. Ebrahimi, A. Khayatiyan, and E.Farjah, "A novel optimizing power control strategy for centralized wind farm control system," *Renewable Energy: An International Journal*, vol. 86, pp. 399-408, 2016.

[22] S. Vedrana, B. Mato, and P. Nedjeljko, "Wind farm load reduction via parametric programming based controller design," *IFAC Proceedings*, vol. 44, no. 1, pp.

1704-1709, 2011.

[23] J. J. B. Berglind, R. Wisniewski, and M. Soltani, "Fatigue load modeling and control for wind turbines based on hysteresis operators," in *Proceedings of IEEE American Control Conference*, Chicago, USA, Jul. 2015, pp. 3721-3727.

[24] S. Huang, Q. Wu, and Y. Guo *et al*., "Hierarchical active power control of DFIG-based wind farm with distributed energy storage systems based on ADMM," *IEEE Transactions on Sustainable Energy*, vol. 11, no. 3, pp. 1528-1538, Jul. 2020.

[25] X. Fan, E. Crisostomi, and D. Thomopulos *et al*., "An optimized decentralized power sharing strategy for wind farm de-loading," *IEEE Transactions on Power Systems*, vol. 36, no. 1, pp. 136-146, Jan. 2021.

[26] C. Mu, T. Ding, and Y. Yuan *et al*., "Decentralized and private solution for the optimal dispatch of integrated wind farms with shared energy storage systems," *IEEE Transactions on Power Systems*, vol. 40, no. 2, pp. 1452-1464, Mar. 2025.

[27] M. A. Bragin, B. Yan, and P. B. Luh, "Distributed and asynchronous coordination of a mixed-integer linear system via surrogate lagrangian relaxation," *IEEE Transactions on Automation Science and Engineering*, vol. 18, no. 3, pp. 1191-1205, Jul. 2021.

[28] J. Hou, Q. Zhai, and Y. Zhou *et al*., "A fast solution method for large-scale unit commitment based on lagrangian relaxation and dynamic programming," *IEEE Transactions on Power Systems*, vol. 39, no. 2, pp. 3130-3140, Mar. 2024.

[29] B. D. Biswas, M. S. Hasan and S. Kamalasadan, "Decentralized distributed convex optimal power flow model for power distribution system based on alternating direction method of multipliers," *IEEE Transactions on Industry Applications*, vol. 59, no. 1, pp. 627-640, Jan. 2023.

[30] M. Moghadam, R. Zhang, and R. Ma, "Distributed frequency control via randomized response of electric vehicles in power grid," *IEEE Transactions on Sustainable Energy*, vol. 7, no. 1, pp. 312-324, Jan. 2016.

[31] J. Morren, S. Haan, and W. L. Kling *et al*., "Wind turbines emulating inertia and supporting primary frequency control," *IEEE Transactions on Power Systems*, vol. 21, no. 1, pp. 433-434, Feb. 2006.

[32] A. THOMMESSEN and C. M. Hackl, "Virtual synchronous machine control for doubly fed induction machine-based wind energy conversion systems," *IEEE Open Journal of the Industrial Electronics Society*, vol. 5, pp. 264-301, Jan. 2024.

[33] J. -S. Kim, Y. -J. Kim, and O. Gomis-Bellmunt *et al*., "Optimal frequency regulation of multi-terminal HVDC-linked grids with deloaded offshore wind farms control," *IEEE Transactions on Sustainable Energy*, vol. 15, no. 1, pp. 290-303, Jan. 2024.

[34] R. K. Subroto, K. L. Lian, and C. -C. Chu *et al*., "A fast frequency control based on model predictive control taking into account of optimal allocation of power from the energy storage system," *IEEE Transactions on Power Delivery*, vol. 36, no. 4, pp. 2467-2478, Aug. 2021.